Scalable Fabrication of Multifunctional Freestanding Carbon Nanotube/Polymer Composite Thin Films for Energy Conversion

Xiaokai Li, Forrest Gittleson, Marcelo Carmo, Ryan C. Sekol, and André D. Taylor*

Chemical & Environmental Engineering Department, Yale University, New Haven, Connecticut 06511, United States

ABSTRACT Translating the unique properties of individual single-walled carbon nanotubes (SWNTs) to the macroscale while simultaneously incorporating additional functionalities into composites has been stymied by inadequate assembly methods. Here we describe a technique for developing multifunctional SWNT/polymer composite thin films that provides a fundamental engineering basis to bridge the gap between their nano- and macroscale properties. Selected polymers are infiltrated into a Mayer rod coated conductive SWNT network to fabricate solar cell transparent conductive electrodes (TCEs), fuel cell membrane electrode assemblies (MEAs), and lithium ion battery electrodes. Our TCEs have an outstanding optoelectronic figure of merit σ_{dc}/σ_{ac} of 19.4 and roughness of 3.8 nm yet are also mechanically robust enough to withstand delamination, a step toward scratch resistance necessary for flexible electronics. Our MEAs show platinum utilization as high as 1550 mW/mg$_{Pt}$, demonstrating our technique's ability to integrate ionic conductivity of the polymer with electrical conductivity of the SWNTs at the Pt surface. Our battery anodes, which show reversible capacity of ~850 mAh/g after 15 cycles, demonstrate the integration of electrode and separator to simplify device architecture and decrease overall weight. Each of these applications demonstrates our technique's ability to maintain the conductivity of SWNT networks and their dispersion within a polymer matrix while concurrently optimizing key complementary properties of the composite. Here, we lay the foundation for the assembly of nanotubes and nanostructured components (rods, wires, particles, *etc.*) into macroscopic multifunctional materials using a low-cost and scalable solution-based processing technique.

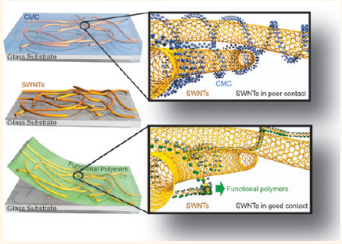

KEYWORDS: carbon nanotube · solar cell · fuel cell · doping · composite · lithium ion battery

Simultaneous optimization of several key functionalities is a fundamental materials science problem. In many cases, there are trade-offs between these properties such that the improvement of one negatively impacts the others. One example of this challenge is in transparent conductive electrodes (TCEs), which require the materials to be highly transparent, electronically conductive, and flexible with a uniformly smooth morphology.[1−3] Thermoelectric devices[4,5] require high electrical conductivity but low thermal conductivity, while good fuel cell catalysts maintain a balance between porosity, ionic, and electrical conductivity. Synthetic multifunctional composites are materials designed and processed to provide multiple performance capabilities in a single system. In the best of such composites, each functionality can be tuned more independently through the manipulation of each corresponding component. For example, fuel cell electrodes[6] typically use a robust ion-conductive polymer (*i.e.*, Nafion), which is mixed with carbon-supported catalysts to provide high surface areas inside of a medium that provides both electronic and ionic pathways.[7] Analogous examples can be found in solar cells,[8−10] electrochemical electrodes,[11,12] sensors, and thermoelectric materials.[5]

Nanostructured materials such as single-walled carbon nanotubes (SWNTs) are particularly attractive as building blocks for these systems due to their unique properties (*i.e.*, high aspect ratio, small diameter, mechanical strength, high electrical/thermal conductivities, and unique optoelectrical properties),[5,13−17] yet maintaining these properties when combined with a polymer to form a composite is challenging. The diffilculty largely stems from the strong van der Waals forces between carbon nanotubes, which leads to poor dispersion of SWNTs in polymer matrices. To improve the nanotubes' solubility, either covalent[18] or noncovalent[19] functionalization approaches have been pursued. In the former, the sidewalls of SWNTs are functionalized with surface moieties that facilitate mixing into a polymeric medium. This approach has shown enhanced

* Address correspondence to andre.taylor@yale.edu.

Received for review October 28, 2011 and accepted January 11, 2012.

Published online January 11, 2012
10.1021/nn2041544

composite mechanical strength due to better dispersion of SWNTs within the polymer matrix as well as a stronger bridge between the polymer and the nanotubes.[20−22] Unfortunately, covalent functionalization creates defects in the nanotube lattice,[23] which can lower the electrical[24] and thermal conductivity of the nanotubes and compromise their mechanical properties. Alternatively, noncovalent functionalization of nanotubes has been shown to preserve nearly all of the individual nanotubes' intrinsic properties;[18] however, the overall composite properties (*i.e.*, electrical, thermal, *etc.*) suffer due to high intertube junction resistance caused by separation of nanotubes by the polymer/surfactant.[25] Such composites have traditionally had low conductivities, typically <10 S/m.[26]

Previously, conductive polymers were employed to disperse CNTs and to minimize the composite resistance. For example, Hellstrom *et al.*[27] and De *et al.*[2] used poly-3-hexylthiophene (P3HT) and poly(3,4-ethylenedioxythiophene):poly(styrenesulfonate) (PEDOT:PSS), respectively, to disperse and deposit uniform carbon nanotube bundle networks for TCEs. Although enhanced optoelectronic performance was achieved due to the improved conductivity, the ability to utilize polymers with other functionalities remains severely limited. In most cases, the electronic conductivity of SWNT networks is severely compromised when nonconductive polymers with other functionalities are incorporated.

The Mayer rod coating method is a scalable technique for making solution-processed thin films in a controlled manner.[28] Fluids that can be effectively coated by the Mayer rod method can often be adapted to more controllable, higher-throughput methods.[3,28] Here we demonstrate a universal technique to fabricate high-performance functional composites containing uniformly dispersed SWNTs within a variety of useful polymer matrices using a tandem Mayer rod casting approach. We first achieve a stable and highly dispersed SWNT suspension that facilitates the Mayer rod coating process. The resulting SWNT networks have better optoelectronic performance than previously reported Mayer rod coated SWNT films and are comparable to the best reported made using any technique. Next, we show that key complementary functionalities can be incorporated into a multifunctional composite without compromising the conductivity of the SWNT network, allowing independent tunability of individual properties. Finally, we characterize the chemical interactions between SWNTs and functional polymers and show how these composite films can be used as key components in solar cells, fuel cells, and batteries.

RESULTS AND DISCUSSION

To fabricate multifunctional composite films, SWNTs are first dispersed using a high molecular weight polymeric derivative of cellulose (sodium carboxymethyl cellulose (CMC)) and then Mayer rod coated onto glass slides. The resulting films are transparent but nonconductive due to the encapsulation of the SWNTs in the CMC polymer matrix (Figure 1a). Samples are then treated with acid to remove the CMC and dope the SWNTs, leading to a denser network with superb electrical contacts between the SWNTs (Figure 1b). Remarkably, as-made films demonstrate higher optoelectronic performance over previously reported Mayer rod coated SWNT films and will be further discussed in the application section. Functional polymers can then be selected based on the intended application and filled into the highly conductive SWNT network. As the polymer occupies the empty space between nanotubes, a freestanding SWNT/polymer multifunctional nanocomposite film can be obtained by peeling off the film from the glass slide (Figure 1c). This method facilitates the combination of SWNTs with various polymers and eliminates a previous requirement for the polymer to be capable of dispersing the SWNTs. In addition, the formation of the SWNT network prior to the incorporation of a functional polymer maintains the superb conductivity of the SWNT network by preventing the presence of polymer between nanotubes. Hence, a highly formed network with low intertube junction resistance results in SWNT/polymer composite films with superb electrical performance.

CMC has been reported as an excellent agent for dispersing SWNTs in water, and transparent films have previously been sprayed;[29] however, this is the first report of CMC-based dispersions for Mayer rod casting of SWNT films. Unlike spray coating, Mayer rod coating of colloidal fluid requires specific rheological behavior and wetting properties.[28,30] The coating fluid should contain enough solid matter to form a uniform and continuous layer upon drying. The coating fluid surface tension should be low enough to facilitate spreading on a wide range of substrates without defects, yet high enough to prevent colloidal agglomeration after deposition. Toward controlling the rheological properties of the coating fluid, Dan *et al.* added Triton X-100 (TX100) to a sodium dodecyl benzenesulfonate (SDBS)-dispersed high-pressure CO conversion (HiPCO) SWNT solution to form flocs which raised the viscosity at low shear velocity by ~3 orders of magnitude.[28] Although this approach facilitated the Mayer rod coating process of HiPCO SWNTs, we found that there are three critical limitations affecting this mixed surfactant system. First, the resulting solution is only stable for a few minutes (Figure 2) before precipitation takes place, which makes it less suitable for industrial applications. Second, the agglomeration of these flocs affects the uniformity and optoelectronic performance of the resulting SWNT films. We illustrate light clusters from an optical microscopy image of a cast film from an SDBS-TX100-HiPCO SWNT dispersion (Figure 2). The existence of these light clusters negatively affects the optoelectronic performance of SWNT networks

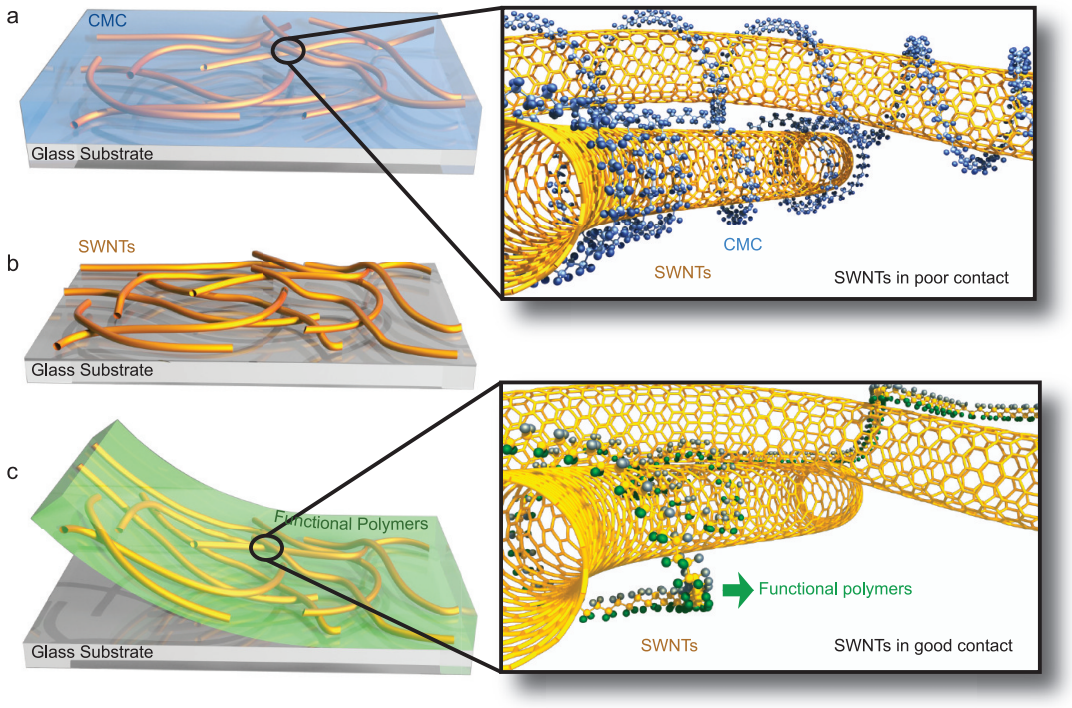

Figure 1. Schematics illustrating the fabrication steps of the polymer/SWNT composites. (a) SWNT/CMC films are made by Mayer rod coating of SWNTs in CMC dispersion on glass substrates. The intertube resistance is very high due the presence of CMC between SWNTs. (b) Acid treatment removes CMC in the Mayer rod casted films, resulting in a densely packed nanotube network. SWNTs are in direct contact with each other. (c) Mayer rod casting of functional polymers results in freestanding multifunctional composite films where the SWNT network is highly conductive.

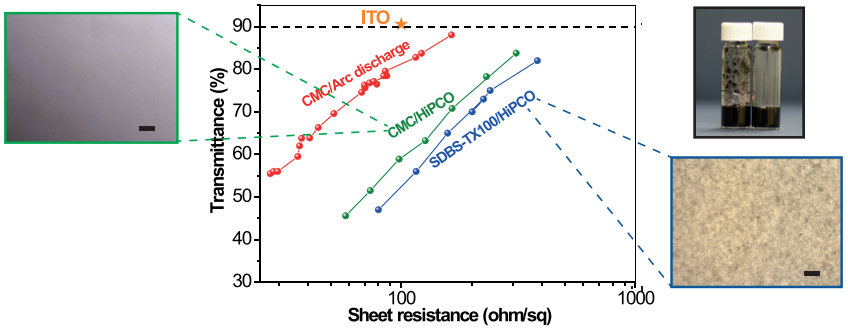

Figure 2. Comparison of the Mayer rod coated SWNT films from various SWNT dispersions. Optoelectronic performance of Mayer rod coated SWNT films: blue, SDBS-TX100/HiPCO; green, CMC/HiPCO; red, CMC/Arc. The photo in black rectangle is (left) a CMC/HiPCO dispersion after 2 weeks and (right) a SDBS-TX100/HiPCO dispersion after 30 min. Agglomeration occurs in the right bottle as flocs can be seen on the vial wall. The light microscope image in green and blue rectangles are, respectively, Mayer rod fabricated SWNT films from (green) CMC/HiPCO dispersion and (blue) SDBS-TX100/HiPCO dispersion. The scale bar is 20 μm.

and can be attributed to the TX100 disturbance of the SDBS/SWNT dispersion. Vigolo *et al.* reported similar large dense clusters from SDS/SWNT dispersions when either insufficient or excessive SDS is present and argued the importance of having a homogeneous dispersion to a film's mechanical strength.[21] Third, the surface chemistry of the SWNTs appears to have a greater effect on stability of the SDBS-TX100 surfactant systems than on the CMC dispersions. For example, it has been reported that arc-discharge (Arc) SWNT networks outperform HiPCO SWNT networks in terms of both optoelectronic performance and lifetime of the final device.[31] Yet, by first dispersing the Arc SWNTs with SDBS followed by adding varying amounts of TX100 (extending the approach of Dan *et al.*), we were unable to achieve the proper rheology to facilitate Mayer rod coating. The SDBS-TX100-Arc SWNT simply would not form a uniform and continuous film for TCE applications. We attribute this observation to the difference in surface chemistry between the Arc SWNTs and the HiPCO SWNTs. Using our approach, we show the achievement of well-dispersed, stable HiPCO and Arc SWNT solutions that have fluid surface tensions low enough to spread on a wide range of substrates yet

high enough to prevent colloidal agglomeration after deposition (Figure 2).

We disperse SWNTs in 3% CMC solution at 1 mg/mL. The shear viscosities of CMC/SWNT dispersions for both HiPCO SWNT and Arc SWNT are compared to an SDBS-TX100/SWNT dispersion (Figure S1 in the Supporting Information).[28] The CMC system exhibits a comparable viscosity at the shear velocity range tested for both HiPCO SWNT and Arc SWNT. This could be due to the high molecular weight of CMC and high surface area of the SWNTs. Figure 2 compares optical microscopy images of as-casted HiPCO SWNT films prepared from SDBS-TX100 and CMC-based dispersions. All films were coated under identical conditions onto a piranha-cleaned glass substrate, as described in the Methods section. We show that films casted from the CMC-based film are optically clear.

CMC readily dissolves in nitric acid, allowing the film to collapse and facilitates the electrically conductive SWNT network formation (Figure 1b). The nitric acid treatment also improves the film properties. The UV−vis absorption spectrum exhibits a significant difference in the S_{22} and M_{11} peaks for a casted SWNT film before and after nitric acid exposure (Figure S2). The suppression of S_{22} and M_{11} peaks after nitric acid soaking indicates p-type doping of the SWNT film.[29]

We compare the optoelectronic performance of films Mayer rod casted from CMC-dispersed HiPCO SWNT dispersion (CMC/HiPCO) and SDBS-TX100-dispersed HiPCO SWNT dispersion (SDBS-TX100/HiPCO) following acid treatment (Figure 2). The CMC/HiPCO films consistently exhibit a better conductivity at all transparency ranges considered. This improved performance could be attributed to the enhanced debundling and stability of the well-dispersed SWNT network from CMC/HiPCO dispersion in comparison to the agglomerated SDBS-TX100/HiPCO dispersion. Figure 2 also compares the optoelectronic performance of the acid-treated HiPCO and arc-discharge SWNT (CMC/Arc) films both casted from CMC dispersion. We have observed that arc-discharged SWNT films consistently exhibit much higher sheet conductance than HiPCO nanotubes by more than one order of magnitude at similar optical transparency, consistent with literature results.[31] The origin of this difference may be related to several factors, including differences in the nanotube dimension, the defect density, the presence of resistive impurities, and the ease of separating bundled nanotubes. These results lay the foundation for building a multifunctional SWNT composite with selected polymers.

To fabricate the multifunctional composite freestanding films, we used a Mayer rod to coat a thin layer of polymer solution onto the acid-treated SWNT network on glass. In a recent paper,[32] Yu *et al.* dropped monomer solution on SWNT films and photopolymerized the monomer to obtain a SWNT/polymer composite. We directly coat functional polymer solutions to maintain the versatility of our tandem Mayer rod coating method. Polyvinyl alcohol (PVA), Nafion, and poly(vinylidene fluoride) (PVDF) were selected due to their contrasting properties and functionalities. We found that the solvent plays a key role during the fabrication process. For example, direct casting of commercially available Nafion solution such as Dupont D1021 on SWNT networks results in films that are very brittle, making it impossible to peel off. Dimethyl sulfoxide (DMSO) solutions consistently yield the highest quality films because DMSO is a polar solvent that dissolves both polar and nonpolar compounds.[33] We found that PVA, Nafion, and PVDF can all be dissolved in DMSO within the required weight concentration (5−20%), which indicates that DMSO is an effective solvent for dissolving these polymers. One advantage of using DMSO over water as the solvent is the lower contact angle (41°) compared to water (114°), allowing it to properly wet the hydrophobic CNTs (Figure S3). This wettability allows the DMSO (and functional polymer) to infiltrate the intertube spaces of the CNT network more effectively than polymer aqueous solutions.[34] DMSO solutions of either PVA, Nafion, or PVDF were Mayer rod casted over the SWNT network, during which process the polymer solution infiltrated through the pores and reached the surface of the glass to form a smooth polymer/glass interface. After drying, the SWNT composite could be peeled off the glass surface to form freestanding polymer/SWNT films (Figure S4).

The described process of first making the SWNT network followed by subsequent filling in with the functional polymer facilitates the evaluation of polymer/SWNT interaction and its effect on the SWNT conductivity. As mentioned previously, the nitric acid treatment dissolves the CMC and p-dopes the SWNTs through the absorption of p-dopant on the SWNT surface. We use a heat treatment (vacuum oven at 150 °C for 24 h) to induce desorption of this p-dopant,[35] which reduces the conductivity of SWNT networks. This drying procedure is typically used as an intermediate step for fabricating the polymer/SWNT composites, and we define these films prior to polymer infiltration as pristine films throughout this paper starting with Figure 3.

The infiltration of PVA, Nafion, and PVDF affects the conductivity of the SWNT network quite differently. As compared to the pristine SWNT films, the sheet resistance of the PVA/SWNT film and the PVDF/SWNTs increases by a factor of 8 and 3, respectively, while the sheet resistance of Nafion/SWNTs slightly decreases (Figure 3a). It has been reported that polymers can dope carbon nanotubes, resulting in a different Fermi level within the carbon nanotube that can improve the intertube junction resistance.[36−38] This resistance change could be attributed to the difference in the electron-donating and -withdrawing capability of these polymers.[39] We show through Raman

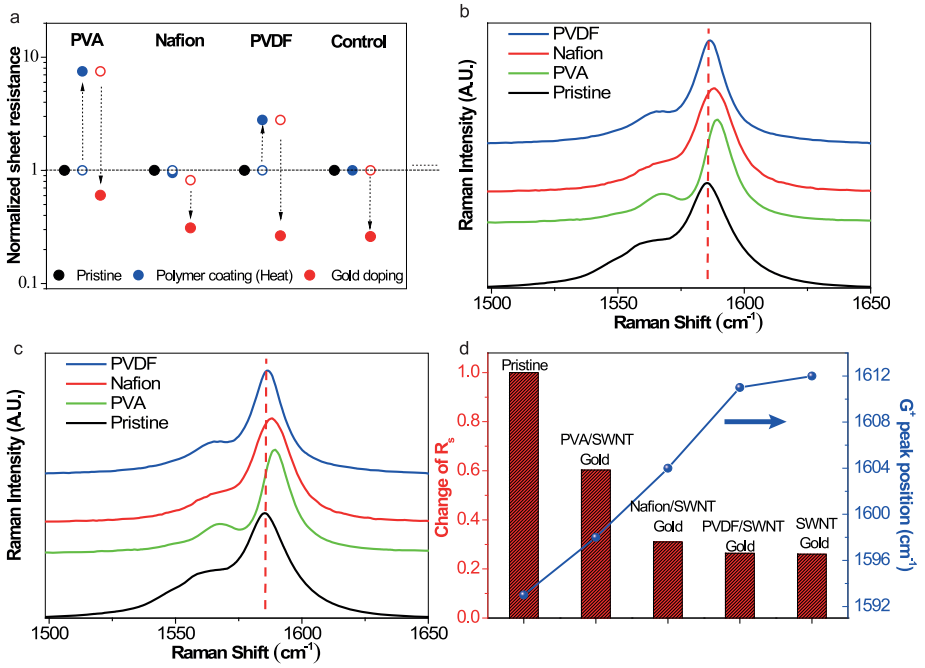

Figure 3. Effect of polymer infiltration as well as gold doping on the properties of SWNT film. (a) Sheet resistance changes with polymer infiltration and gold doping. Raman shifts of pristine SWNTs and polymer/SWNT composite materials with excitation energy of (b) 2.33 eV and (c) 1.58 eV. (d) Relationship between G-band peak position and sheet resistance change of the composite film. A laser with an excitation energy of 2.33 eV was used.

spectroscopy (Figure 3b,c) that the G-band appears near 1593 cm^{-1} for pristine SWNT films. The peak positions of the G-band are not shifted appreciably with the infiltration of PVDF and are upshifted by about 3 cm^{-1} with the infiltration of PVA and Nafion. This upshift can be attributed to the phonon stiffening effect by p-type doping.[40] The slight sheet resistance reduction in Nafion/SWNT film could result from Nafion p-doping of the SWNTs. The reason for the increase in sheet resistance after infiltration of PVA and PVDF is not entirely clear. We speculate that this may be related to the crystallinity of the polymer. We performed differential scanning calorimetry (DSC) to study the crystallinity of the three polymer/composite systems. As shown in Supporting Information Figure S5, given the exact same casting condition, the crystallinity of PVA/SWNT composite films is higher than that of pure PVA films. It has been reported that the crystallinity of PVA increases linearly with carbon nanotube content,[20] and this linearity is a signature of nucleation of local polymer crystallinity by the nanotube. This PVA crystalline coating around the nanotube could improve the load transfer from PVA to SWNTs when PVA films are stretched and will increase the modulus of PVA/SWNT films.[20] In the meantime, it could also affect the tube−tube contacts, resulting in an increased resistance across the SWNT network. The PVDF film shows similar crystalline-promoting phenomena, while Nafion films do not show any crystallinity. The crystallinity change with and without SWNTs correlates with the sheet resistance change before and after the infiltration of polymers. We believe that these freestanding SWNT composites could potentially be used in the next generation of flexible electronics. It is noteworthy to mention that flexible electronics are expected to be bent, scratched, stretched, and compressed extensively. The polymer SWNT interaction we observed could improve the flexible durability of these devices but lower the overall conductivity of the network. We show that the conductivity can be recovered through gold doping.

To further improve the conductivity of the polymer/SWNT composites, the freestanding films were treated with $HAuCl_4$ (Au^{3+}) dissolved in nitromethane. The Fermi level of a SWNT is well above the reduction potentials of $AuCl_4^-$, which results in spontaneous electron transfer from the nanotube (p-doping) to the metal ions and promotes their reduction and formation of gold nanoparticles on SWNT surfaces.[41] This dramatically reduces the intertube junction resistance,[42] and we show (Figure 3a) that the sheet resistance for all three polymer/SWNT systems significantly decreased. The resistance of gold-doped PVDF/SWNT film is the lowest among the three and is very close to the control (gold-doped pristine SWNTs on a glass substrate), followed by the gold-doped Nafion/SWNTs and gold-doped PVA/SWNT systems. There is a very strong correlation between the G-band positions of these films and their sheet resistance (Figure 3d). For instance, a larger reduction in the sheet resistance corresponds to an upshift in G peak position. This indicates that the presence of polymer significantly affects the possibility of gold reduction on the SWNT surface.

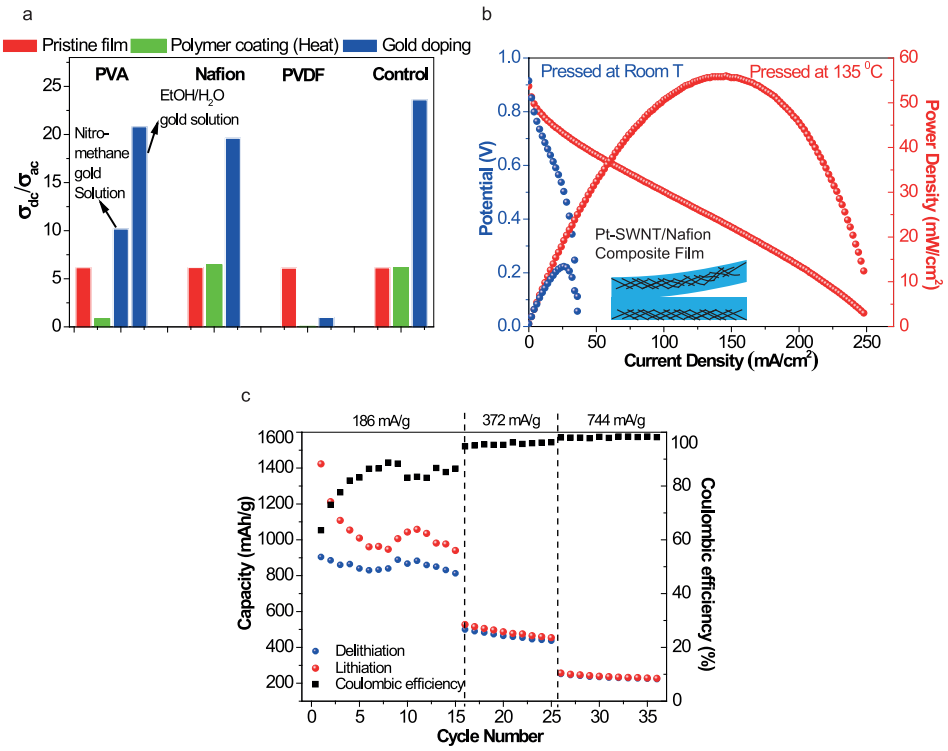

Figure 4. Application of polymer/SWNT composite films. (a) Values of σ_{dc}/σ_{ac} of our Mayer rod casted before and after polymer infiltration as well as σ_{dc}/σ_{ac} value changes before and after gold doping for all films. (b) Performance of the MEA by Nafion to Nafion hot pressing two Nafion/SWNT-Pt films with anode and cathode loadings of 0.018 mg_{Pt}/cm^2 each. (c) Lithiation (red) and delithiation (blue) capacity and Coulombic efficiency (black) *versus* cycle number for Nafion/SWNT electrodes at 186, 372, and 744 mA/g. The SWNT loading density of the film is 0.036 mg/cm^2.

PVA has actually been rated to have excellent resistance to permeation of nitromethane and thus is very likely to prevent the gold salt in nitromethane from reaching the SWNT surface toward p-doping the SWNTs. We performed contact angle measurements to indirectly evaluate the wettability and permeability of nitromethane on the three polymer/SWNT systems and the bare SWNT film. A drop of nitromethane gold solution is dropped on the film surface, and snapshots are taken at 10 s, 1 min, and 2 min intervals until the droplet disappears (Figure S6). Under the same conditions, we reveal that the faster a droplet disappears, the better the nitromethane permeation and improved conductivity *via* p-doping of SWNTs in that film. The order of decreasing permeation was the following: SWNTs on glass, PVDF/SWNTs, Nafion/SWNTs, and PVA/SWNTs. These observations are consistent with the Raman shift and sheet resistance reduction outcomes. This suggests that improvements in the conductivity of PVA/SWNT and Nafion/SWNT composite films can be realized through proper selection of solvents. To validate this point, we treated PVA/SWNT composite film with gold salt in ethanol/water (50/50), where ethanol/water could very easily permeate PVA. Similar sheet resistance reduction in PVA/SWNT composite upon gold doping was observed as that for pristine SWNT films on glass. This solvent effect is shown in Figure 4a, and the figure of merit will be discussed shortly.

We present the morphologies of pristine SWNTs (Figure S7) on glass and three freestanding polymer/SWNT composite films, before and after gold doping from Au^{3+} nitromethane solution. SEM micrographs reveal that the polymers infiltrate between SWNTs. The resulting SWNT networks appear to be smoother than bare SWNTs with all the spaces in the bare films filled in by selected polymers. Gold nanoparticles grow with the immersion of SWNT film and polymer/SWNT films in gold salt solution. We demonstrate (Figure S7) that nanoparticles can be observed for the Nafion/SWNT and PVDF/SWNT films but not for the PVA/SWNTs, which is also consistent with the conductivity results (Figure 3a).

We evaluated the composite freestanding films as replacements for ITO in organic light-emitting diode and organic solar cell anodes. The most important parameters for evaluating the performance of transparent electrodes are generally the transparency and the sheet resistance. However, since the sheet resistance of the SWNT film is strongly dependent upon the transparency, it is not informative to directly compare each property of SWNT films. It has been suggested[43] that the ratio of the direct current conductivity, σ_{dc}, to the optical conductivity, σ_{ac} (typically at 550 nm), be considered as a figure of merit (FOM) and that a higher value of the σ_{dc}/σ_{ac} ratio indicates improved performance of the SWNT network. This FOM comes from the relationship with transparency, T, and sheet resistance, R_s, as given by

TABLE 1. Optoelectronic Performance of SWNT Film Comparison

surfactant	method	surface roughness (nm)	substrate	σ_{dc}/σ_{ac}	ref
PSS[a]	LBL[b]		glass	18.8	44
SPEEK[c]	LBL	3.5	glass/PET	2.8	39
5TN-PEG[d]	spin		glass	17	45
rr-P3HT[e]	spin	12	glass	13	27
SDS[f]	spray	9	PET	24	46
Nafion	spray	10	PET	16	47
CMC	spray	3	glass	9.5	29
PEDOT:PSS[g]	VF		PET	15	2
SDS	VF	3.1	glass/PE	16	31
SDBS+TX100[h]	Mayer rod		glass	13	28
CMC	Mayer rod	12.1	glass	24	this work
CMC	Mayer rod	3.8	freestanding	19.4	this work

[a] Poly(styrene sulfonate). [b] Layer by layer. [c] Sulfonated polyether ether ketone. [d] Quinquethiophene-terminated poly(ethylene glycol). [e] Poly(3-hexylthiophene). [f] Sodium dodecyl sulfate. [g] Poly(3,4-ethylenedioxythiophene):poly(styrene sulfonate). [h] Triton X-100.

$$T = \left(1+\frac{2\pi}{cR_s}\frac{\sigma_{ac}}{\sigma_{dc}}\right)^{-2}$$

We show (Figure 4a) that Nafion/SWNT films exhibited a σ_{dc}/σ_{ac} ratio of 19.4, while PVA/SWNT composite films have a FOM as high as 20.8. The latter FOM is a result of proper solvent selection for the gold doping process. PVDF/SWNT films have a low figure of merit due to the poor transmittance of PVDF. Table 1 compares our results with other reported data for SWNT films. Our SWNT films on glass as well as freestanding polymer/SWNT composite films exhibit optoelectronic performance that competes with the best reported data in literature. This opens up the opportunity of utilizing these composite films for many other applications. In addition, the AFM results show that the surface roughness of the Nafion/SWNT undoped and doped films are 3.2 and 3.8 nm root mean square (rms), respectively. Prior to Nafion infiltration, the rms roughness of the pristine films on glass substrates was 11.2 and 12.1 nm before and after gold doping, respectively (Figure 5). The insets in Figure 5 are close up height (left) and phase (right) AFM images of the corresponding films. The phase images discriminate between different types of materials on the surface. The dark particles shown in Figure 5d (right inset) are gold nanoparticles. We also confirm that these composite films are scratch-resistant based on scotch tape evaluations (Figure S8). Due to the versatility of our method, we could expect to easily incorporate other desirable functionalities (such as mechanical strength and low oxygen permeability) into our TCEs by proper selection and combination of functional polymers. Below are a few examples of how this functionality can be applied to fuel cells and lithium-based batteries.

A key challenge toward the commercialization of proton-exchange membrane (PEM) fuel cells is the cost. One of the primary cost-drivers is the membrane electrode assembly (MEA), which consists of the catalysts, electrolyte membrane, and gas diffusion layers (GDLs). Reducing PEM fuel cell cost and improving performance will require more efficient utilization of the catalyst and a reduction in the overall thickness of the MEA, which requires optimization of the system architecture.[6,48] Traditional solution processing of the MEA requires special care during synthesis to avoid isolated SWNT-Pt agglomerations, where the Pt cannot contribute to electrochemical conversion reactions. Using our method, the formation of highly conductive SWNT networks first, followed by infiltration of an ionically conductive phase, may dramatically increase the accessibility of Pt to both the electronic and ionic carriers and thus yield a higher Pt utilization. In addition, the catalytic layer thickness can be easily controlled using the Mayer rod method to optimize the structure of the membrane electrode assembly. We demonstrate the assembly of an MEA by simply pressing together the Nafion sides of two Mayer rod coated Nafion/SWNT films (Figure 4b inset).

We report that the polymer infiltration step can be used to create films that are conductive only on the SWNT network side. For the fuel cell MEA demonstration, Pt-decorated SWNTs (SWNT-Pt) were synthesized by a supercritical method developed in our lab.[49] Nafion/SWNT-Pt composite films were obtained first by Mayer rod casting of the SWNT-Pt dispersion, followed by acid treatment to remove the CMC. Nafion was then infiltrated into the SWNT-Pt network in excess to create an anisotropic film (Figure 4b inset). We show fuel cell performance results (Figure 4b) for an MEA with Pt loading of 0.018 mg/cm^2 at both the anode and cathode. A peak power density of 55.8 mW/cm^2 gives a platinum utilization of 1550 mW/mg$_{Pt}$ after hot pressing at 135 °C. Conventional fuel cells typically exhibit an overall Pt utilization of ~400 mW/mg$_{Pt}$.[7] As indicated in Figure 4b, pressing is a crucial step in fusing the two Nafion films together to form a continuous Nafion phase that facilitates the ion transportation. We note that the results for these MEAs are not optimized; yet they demonstrate a new and novel approach for fuel cell MEA assembly.

In recent years, great attention has been paid to the use of carbon nanotubes for lithium ion batteries.[50] Reversible capacities exceeding a LiC_2 stoichiometry (>1116 mAh/g) are proposed for SWNTs, representing a dramatic improvement over conventional graphite anodic capacity.[51] Our Nafion/SWNT film with its dual-purpose integrated architecture was evaluated as a combined lithium ion battery anode and separator. Here, the SWNTs behave as the active anode material while Nafion offers mechanical strength to the SWNT electrode and serves as a barrier between the anode and the lithium counter electrode. A reversible capacity of ~850 mAh/g was achieved after 15 cycles at a charge/discharge rate of 186 mA/g (Figure 4c). Upon further cycling at the increased rates of 372 and 744 mA/g, the reversible capacity dropped significantly

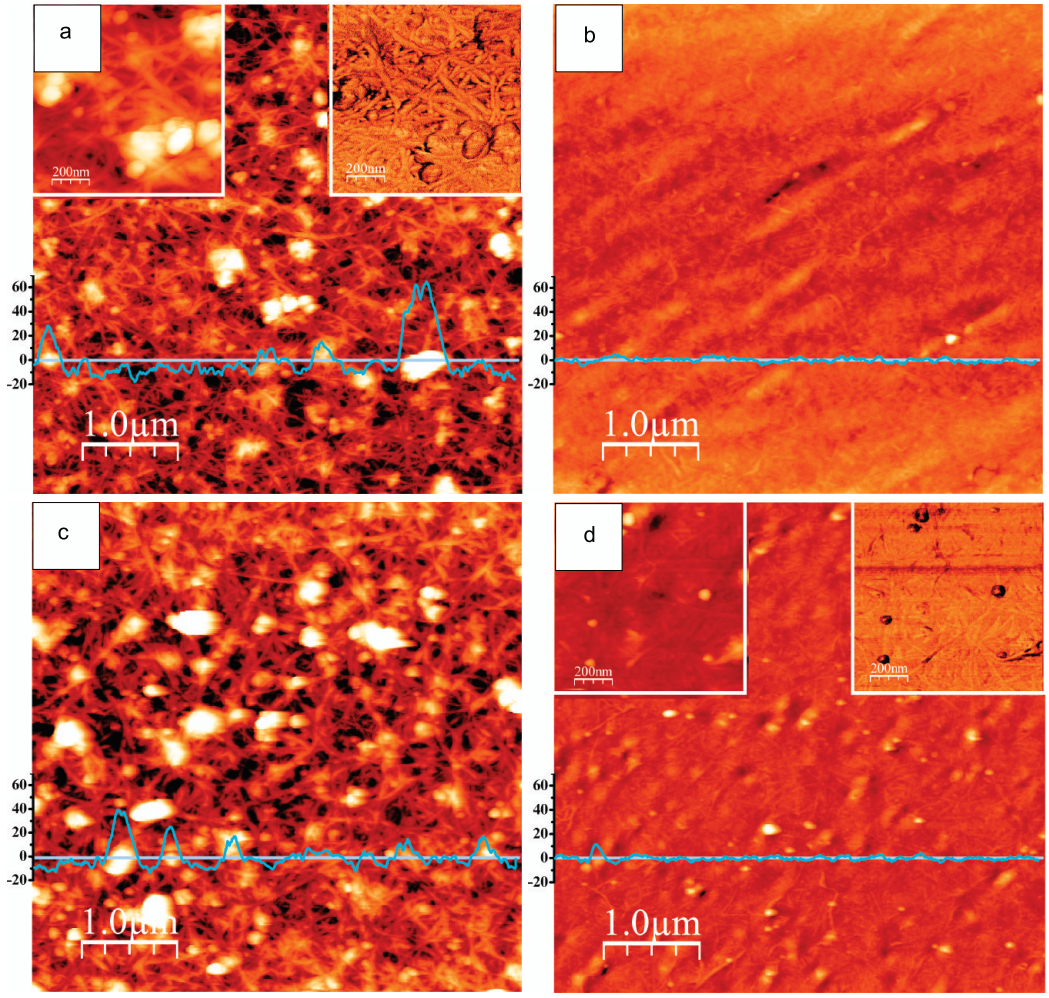

Figure 5. Surface morphorlogy of pristine SWNT film on glass and freestanding SWNT/Nafion composite film. AFM image of (a) pristine SWNT film, (b) SWNT films infiltrated by Nafion and their corresponding gold-doped SWNT films. (c) SWNT on glass after gold doping and (d) Nafion/SWNTs after gold doping. The roughness of the films is as follows: (a) 11.2 nm, (b) 3.2 nm, (c) 12.1 nm, (d) 3.8 nm.

as a consequence of poor film stability in the organic solvent-containing electrolyte. Using the facile Mayer rod method, this unique integrated battery architecture can be extended to produce a solid polymer electrolyte battery in which the same SWNT anode is united with a blend of ion-conducting polymer and lithium salt that serves as both an electrolyte and a separator, thus eliminating the need for a liquid electrolyte. This revised architecture could eliminate capacity degradation due to liquid electrolyte decomposition and improve the safety profile by reducing the chance of cross-electrode shorting. We posit that further improvements in the ion conduction at the electrode/electrolyte interface can be achieved by using optimized polymers and blends. This simple process facilitates a flexible battery design with possible improvements in capacity, stability, and safety.

CONCLUSION

In summary, we have developed and demonstrated a scalable method of producing multifunctional SWNT/polymer composite thin films. As the challenges of generating more complex SWNT-based film systems require engineers to impart new and transformative functionalities to materials without sacrificing the conductivity or ease of manufacturing, our technique provides the versatility to control nanoscale features and functionality on the macroscopic level.

METHODS

Arc-discharge carbon nanotubes are purchased from ILJIN Nanotech, grade ASP-100F, while high-pressure CO conversion (HiPCO) SWNTs are kindly provided by Southwest Nanotechnologies. Ten milligrams of the tubes is mixed with 300 mg of sodium carboxymethyl cellulose (90 000 MW, Sigma Aldrich) and 10 mL of DI water. Solutions are sonicated for 15 min, using a 1/4 in. probe sonicator operated at 225 W (Cole Parmer Model CPX 750, 20 kHz). Solutions are then centrifuged at 8500 rpm for 2 h, and

the final dispersions are obtained by decanting the top 60% of the supernatant. The SDBS/Triton X-100 dispersion is prepared as described by Dan *et al.*[28]

To deposit a SWNT film, 300 μL of the SWNT dispersion is dropped on a piranha-cleaned glass substrate. Then, a Mayer rod (RD Specialist Inc.) is rolled over the solution, leaving a uniform, thin layer of SWNT dispersion on the substrate. Then, the wet coating of the SWNT on glass is carefully dried using a lamp. Samples are placed in 9 M HNO_3 overnight to remove surfactant and dope the networks. After removal from the acid bath, the samples are air-dried without rinsing.

PVA, Nafion, and PVDF of 5−10 wt % in DMSO are then dropped on the as-made SWNT film on a glass slide. A Mayer rod is then rolled over the solution, leaving a wet polymer film over the SWNT networks. Wet films are dried in a vacuum oven at 85 °C for 2 h. Dried films (Nafion is further heated in the oven at 120 °C for another hour) can be readily peeled off from the glass slide, generating a freestanding SWNT/polymer film.

Fuel Cell Test. Pt is loaded on the SWNT by a supercritical fluid method (SC) previously developed in our lab:[49] In a 4.1 mL stainless steel reactor, SWNTs (35.0 mg), platinum(II) acetylacetonate (87.5 mg), and methanol (3.28 mL) are combined. The contents are sealed and placed into a sand bath at 300 °C for 30 min. Under these conditions, the MeOH becomes a supercritical fluid capable of reducing the platinum(II) acetylacetonate. This formulation results in a Pt-SWNT catalyst that has a nominal loading of 55 wt % Pt. The Pt-SWNT is then filtered and rinsed several times in ethanol and dried at 60−80 °C under vacuum for 24 h. The actual loading of Pt on SWNT is determined by TGA to be 42%. Twenty milligrams of Pt-SWNT and 300 mg of CMC are mixed in 10 mL of DI water. The mixture is tip sonicated for 15 min but is not centrifuged. Pt-SWNT/Nafion films are fabricated on 2 in. by 3 in. glass slides using the as-made dispersion the same way SWNT/Nafion composite films are fabricated. Fuel cell MEAs are then generated by pressing two Pt-SWNT/Nafion films together with the Nafion sides facing each other and carbon nanotube sides facing outside. The Pt loading on both anode and cathode sides are 0.018 mg/cm^2. The MEAs are tested in single fuel cell housing and are conditioned overnight until a steady state current is achieved at a potential of 0.6 V. The temperature of the fuel cell is 80 °C, and the anode and cathode saturators are set at 85 °C. The flow rates of the humidified hydrogen and oxygen are set at 100 sccm. An Agilent electronic load controlled the cell potential, and a National Instruments data acquisition system controlled the inputs.

Electrochemical Characterization. Electrochemical measurements have been studied in a Swagelok cell (half-cell). The complete cell preparation steps are performed in an argon glovebox. A pure Li (purity, 99.9%) metal foil is used as a counter electrode, while the Nafion/SWNT composite freestanding film is used as an integration of working electrode and separator. The Swagelok cells used 1.0 M $LiPF_6$ in EC-DMC (1:1 in volume) (ethylene carbonate/dimethyl carbonate) as the electrolyte.

Instrumentation. Sheet resistance measurements are performed using a Signatone four-point probe with 10 mil radius contacts and 40 mil spacing. A Keithley Model 2400 SourceMeter is used to apply current and measure the resulting potential drop. Voltage drop is measured with applied currents and converted to a sheet resistance using $[\pi/\ln 2] \times V/I \cong 4.53 \times V/I$. Atomic force microscopy is taken using a Veeco Dimension 5000 in tapping mode. A Hitachi SU-70 SEM is employed to visually characterize the film. Raman spectra are collected on a Jasco NRS-3100 laser Raman spectrometer with excitation wavelengths of 532 and 785 nm. Bulk rheological experiments are conducted on a strain-controlled rheometer (TA Orchestrator). Contact angle is measured using VCA 2500 MA (AST Products, Inc.). Differential scanning calorimetry is conducted using a TA Instruments Q200.

Acknowledgment. Financial support for this work came from the Semiconductor Research Corporation 2011-RJ-21516 and National Science Foundation NSF-CBET-0954985 CAREER Award. We thank Southwest Nanotechnologies for providing us HiPCO SWNTs, the Pfefferle Group for the use of their Raman spectroscopy, and Z. Shao from the Osuji lab for rheological experiments.

Supporting Information Available: Additional experimental results including UV−vis spectra, contact angle, SEM, and scotch tape test results. This material is available free of charge *via* the Internet at http://pubs.acs.org.

REFERENCES AND NOTES

1. Kumar, A.; Zhou, C. W. The Race To Replace Tin-Doped Indium Oxide: Which Material Will Win? *ACS Nano* **2010**, *4*, 11–14.
2. De, S.; Lyons, P. E.; Sorel, S.; Doherty, E. M.; King, P. J.; Blau, W. J.; Nirmalraj, P. N.; Boland, J. J.; Scardaci, V.; Joimel, J.; *et al.* Transparent, Flexible, and Highly Conductive Thin Films Based on Polymer−Nanotube Composites. *ACS Nano* **2009**, *3*, 714–720.
3. Hu, L. B.; Kim, H. S.; Lee, J. Y.; Peumans, P.; Cui, Y. Scalable Coating and Properties of Transparent, Flexible, Silver Nanowire Electrodes. *ACS Nano* **2010**, *4*, 2955–2963.
4. Leclerc, M.; Najari, A. Organic Thermoelectrics Green Energy from a Blue Polymer. *Nat. Mater.* **2011**, *10*, 409–410.
5. Kim, D.; Kim, Y.; Choi, K.; Grunlan, J. C.; Yu, C. H. Improved Thermoelectric Behavior of Nanotube-Filled Polymer Composites with Poly(3,4-ethylenedioxythiophene) Poly(styrenesulfonate). *ACS Nano* **2010**, *4*, 513–523.
6. Taylor, A. D.; Michel, M.; Sekol, R. C.; Kizuka, J. M.; Kotov, N. A.; Thompson, L. T. Fuel Cell Membrane Electrode Assemblies Fabricated by Layer-by-Layer Electrostatic Self-Assembly Techniques. *Adv. Funct. Mater.* **2008**, *18*, 3003–3009.
7. Taylor, A. D.; Kim, E. Y.; Humes, V. P.; Kizuka, J.; Thompson, L. T. Inkjet Printing of Carbon Supported Platinum 3-D Catalyst Layers for Use in Fuel Cells. *J. Power Sources* **2007**, *171*, 101–106.
8. Kongkanand, A.; Dominguez, R. M.; Kamat, P. V. Single Wall Carbon Nanotube Scaffolds for Photoelectrochemical Solar Cells. Capture and Transport of Photogenerated Electrons. *Nano Lett.* **2007**, *7*, 676–680.
9. Ham, M. H.; Paulus, G. L. C.; Lee, C. Y.; Song, C.; Kalantar-zadeh, K.; Choi, W.; Han, J. H.; Strano, M. S. Evidence for High-Efficiency Exciton Dissociation at Polymer/Single-Walled Carbon Nanotube Interfaces in Planar Nano-heterojunction Photovoltaics. *ACS Nano* **2010**, *4*, 6251–6259.
10. Rahman, G. M. A.; Guldi, D. M.; Cagnoli, R.; Mucci, A.; Schenetti, L.; Vaccari, L.; Prato, M. Combining Single Wall Carbon Nanotubes and Photoactive Polymers for Photoconversion. *J. Am. Chem. Soc.* **2005**, *127*, 10051–10057.
11. Hou, Y.; Cheng, Y. W.; Hobson, T.; Liu, J. Design and Synthesis of Hierarchical MnO_2 Nanospheres/Carbon Nanotubes/Conducting Polymer Ternary Composite for High Performance Electrochemical Electrodes. *Nano Lett.* **2010**, *10*, 2727–2733.
12. Kaempgen, M.; Chan, C. K.; Ma, J.; Gruner, G.; Cui, Y. Printable Thin Film Supercapacitors Using Single-Walled Carbon Nanotubes. *Nano Lett.* **2009**, *9*, 1872–1876.
13. Baughman, R. H.; Zakhidov, A. A.; de Heer, W. A. Carbon Nanotubes: The Route toward Applications. *Science* **2002**, *297*, 787–792.
14. Yu, M. F.; Lourie, O.; Dyer, M. J.; Moloni, K.; Kelly, T. F.; Ruoff, R. S. Strength and Breaking Mechanism of Multiwalled Carbon Nanotubes under Tensile Load. *Science* **2000**, *287*, 637–640.
15. Fuhrer, M. S.; Nygard, J.; Shih, L.; Forero, M.; Yoon, Y. G.; Mazzoni, M. S. C.; Choi, H. J.; Ihm, J.; Louie, S. G.; Zettl, A.; *et al.* Crossed Nanotube Junctions. *Science* **2000**, *288*, 494–497.
16. Mamedov, A. A.; Kotov, N. A.; Prato, M.; Guldi, D. M.; Wicksted, J. P.; Hirsch, A. Molecular Design of Strong Single-Wall Carbon Nanotube/Polyelectrolyte Multilayer Composites. *Nat. Mater.* **2002**, *1*, 190–194.
17. Tans, S. J.; Verschueren, A. R. M.; Dekker, C. Room-Temperature Transistor Based on a Single Carbon Nanotube. *Nature* **1998**, *393*, 49–52.
18. Tasis, D.; Tagmatarchis, N.; Bianco, A.; Prato, M. Chemistry of Carbon Nanotubes. *Chem. Rev.* **2006**, *106*, 1105–1136.
19. Islam, M. F.; Rojas, E.; Bergey, D. M.; Johnson, A. T.; Yodh, A. G. High Weight Fraction Surfactant Solubilization of

Single-Wall Carbon Nanotubes in Water. *Nano Lett.* **2003**, *3*, 269–273.
20. Coleman, J. N.; Cadek, M.; Blake, R.; Nicolosi, V.; Ryan, K. P.; Belton, C.; Fonseca, A.; Nagy, J. B.; Gun'ko, Y. K.; Blau, W. J. High-Performance Nanotube-Reinforced Plastics: Understanding the Mechanism of Strength Increase. *Adv. Funct. Mater.* **2004**, *14*, 791–798.
21. Vigolo, B.; Penicaud, A.; Coulon, C.; Sauder, C.; Pailler, R.; Journet, C.; Bernier, P.; Poulin, P. Macroscopic Fibers and Ribbons of Oriented Carbon Nanotubes. *Science* **2000**, *290*, 1331–1334.
22. Ajayan, P. M.; Tour, J. M. Materials Science - Nanotube Composites. *Nature* **2007**, *447*, 1066–1068.
23. Park, H.; Zhao, J. J.; Lu, J. P. Effects of Sidewall Functionalization on Conducting Properties of Single Wall Carbon Nanotubes. *Nano Lett.* **2006**, *6*, 916–919.
24. Strano, M. S.; Dyke, C. A.; Usrey, M. L.; Barone, P. W.; Allen, M. J.; Shan, H. W.; Kittrell, C.; Hauge, R. H.; Tour, J. M.; Smalley, R. E. Electronic Structure Control of Single-Walled Carbon Nanotube Functionalization. *Science* **2003**, *301*, 1519–1522.
25. Geng, H. Z.; Lee, D. S.; Kim, K. K.; Han, G. H.; Park, H. K.; Lee, Y. H. Absorption Spectroscopy of Surfactant-Dispersed Carbon Nanotube Film: Modulation of Electronic Structures. *Chem. Phys. Lett.* **2008**, *455*, 275–278.
26. Bauhofer, W.; Kovacs, J. Z. A Review and Analysis of Electrical Percolation in Carbon Nanotube Polymer Composites. *Compos. Sci. Technol.* **2009**, *69*, 1486–1498.
27. Hellstrom, S. L.; Lee, H. W.; Bao, Z. N. Polymer-Assisted Direct Deposition of Uniform Carbon Nanotube Bundle Networks for High Performance Transparent Electrodes. *ACS Nano* **2009**, *3*, 1423–1430.
28. Dan, B.; Irvin, G. C.; Pasquali, M. Continuous and Scalable Fabrication of Transparent Conducting Carbon Nanotube Films. *ACS Nano* **2009**, *3*, 835–843.
29. Tenent, R. C.; Barnes, T. M.; Bergeson, J. D.; Ferguson, A. J.; To, B.; Gedvilas, L. M.; Heben, M. J.; Blackburn, J. L. Ultrasmooth, Large-Area, High-Uniformity, Conductive Transparent Single-Walled-Carbon-Nanotube Films for Photovoltaics Produced by Ultrasonic Spraying. *Adv. Mater.* **2009**, *21*, 3210.
30. Hu, L. B.; Hecht, D. S.; Gruner, G. Carbon Nanotube Thin Films: Fabrication, Properties, and Applications. *Chem. Rev.* **2010**, *110*, 5790–5844.
31. Zhang, D. H.; Ryu, K.; Liu, X. L.; Polikarpov, E.; Ly, J.; Tompson, M. E.; Zhou, C. W. Transparent, Conductive, and Flexible Carbon Nanotube Films and Their Application in Organic Light-Emitting Diodes. *Nano Lett.* **2006**, *6*, 1880–1886.
32. Yu, Z.; Niu, X.; Liu, Z.; Pei, Q. Intrinsically Stretchable Polymer Light-Emitting Devices Using Carbon Nanotube–Polymer Composite Electrodes. *Adv. Mater.* **2011**, *23*, 3989.
33. Zeng, X. Y.; Zhang, Q. K.; Yu, R. M.; Lu, C. Z. A New Transparent Conductor: Silver Nanowire Film Buried at the Surface of a Transparent Polymer. *Adv. Mater.* **2010**, *22*, 4484–4488.
34. Liu, K.; Sun, Y. H.; Lin, X. Y.; Zhou, R. F.; Wang, J. P.; Fan, S. S.; Jiang, K. L. Scratch-Resistant, Highly Conductive, and High-Strength Carbon Nanotube-Based Composite Yarns. *ACS Nano* **2010**, *4*, 5827–5834.
35. Jackson, R.; Domercq, B.; Jain, R.; Kippelen, B.; Graham, S. Stability of Doped Transparent Carbon Nanotube Electrodes. *Adv. Funct. Mater.* **2008**, *18*, 2548–2554.
36. Engtrakul, C.; Davis, M. F.; Gennett, T.; Dillon, A. C.; Jones, K. M.; Heben, M. J. Protonation of Carbon Single-Walled Nanotubes Studied Using ^{13}C and ^{1}H-^{13}C Cross Polarization Nuclear Magnetic Resonance and Raman Spectroscopies. *J. Am. Chem. Soc.* **2005**, *127*, 17548–17555.
37. Wang, S.; Yu, D.; Dai, L. Polyelectrolyte Functionalized Carbon Nanotubes as Efficient Metal-Free Electrocatalysts for Oxygen Reduction. *J. Am. Chem. Soc.* **2011**, *133*, 5182–5185.
38. Mistry, K. S.; Larsen, B. A.; Bergeson, J. D.; Barnes, T. M.; Teeter, G.; Engtrakul, C.; Blackburn, J. L. n-Type Transparent Conducting Films of Small Molecule and Polymer Amine Doped Single-Walled Carbon Nanotubes. *ACS Nano* **2011**, *5*, 3714–3723.
39. Zhu, J.; Shim, B. S.; Di Prima, M.; Kotov, N. A. Transparent Conductors from Carbon Nanotubes LBL-Assembled with Polymer Dopant with $\pi-\pi$ Electron Transfer. *J. Am. Chem. Soc.* **2011**, *133*, 7450–7460.
40. Rao, A. M.; Eklund, P. C.; Bandow, S.; Thess, A.; Smalley, R. E. Evidence for Charge Transfer in Doped Carbon Nanotube Bundles from Raman Scattering. *Nature* **1997**, *388*, 257–259.
41. Choi, H. C.; Shim, M.; Bangsaruntip, S.; Dai, H. J. Spontaneous Reduction of Metal Ions on the Sidewalls of Carbon Nanotubes. *J. Am. Chem. Soc.* **2002**, *124*, 9058–9059.
42. Kim, K. K.; Bae, J. J.; Park, H. K.; Kim, S. M.; Geng, H. Z.; Park, K. A.; Shin, H. J.; Yoon, S. M.; Benayad, A.; Choi, J. Y.; *et al.* Fermi Level Engineering of Single-Walled Carbon Nanotubes by $AuCl_3$ Doping. *J. Am. Chem. Soc.* **2008**, *130*, 12757–12761.
43. Hu, L.; Hecht, D. S.; Gruner, G. Percolation in Transparent and Conducting Carbon Nanotube Networks. *Nano Lett.* **2004**, *4*, 2513–2517.
44. Shim, B. S.; Zhu, J. A.; Jan, E.; Critchley, K.; Kotov, N. A. Transparent Conductors from Layer-by-Layer Assembled SWNT Films: Importance of Mechanical Properties and a New Figure of Merit. *ACS Nano* **2010**, *4*, 3725–3734.
45. Jo, J. W.; Jung, J. W.; Lee, J. U.; Jo, W. H. Fabrication of Highly Conductive and Transparent Thin Films from Single-Walled Carbon Nanotubes Using a New Non-ionic Surfactant *via* Spin Coating. *ACS Nano* **2010**, *4*, 5382–5388.
46. Geng, H. Z.; Kim, K. K.; So, K. P.; Lee, Y. S.; Chang, Y.; Lee, Y. H. Effect of Acid Treatment on Carbon Nanotube-Based Flexible Transparent Conducting Films. *J. Am. Chem. Soc.* **2007**, *129*, 7758.
47. Geng, H. Z.; Kim, K. K.; Song, C.; Xuyen, N. T.; Kim, S. M.; Park, K. A.; Lee, D. S.; An, K. H.; Lee, Y. S.; Chang, Y.; *et al.* Doping and De-doping of Carbon Nanotube Transparent Conducting Films by Dispersant and Chemical Treatment. *J. Mater. Chem.* **2008**, *18*, 1261–1266.
48. Michel, M.; Taylor, A.; Sekol, R.; Podsiadlo, P.; Ho, P.; Thompson, L.; Kotov, N. High-Performance Nanostructured Membrane Electrode, Assemblies for Fuel Cells Made by Layer-By-Layer Assembly of Carbon Nanocolloids. *Adv. Mater.* **2007**, *19*, 3859.
49. Taylor, A. D.; Sekol, R. C.; Kizuka, J. M.; D'Cunha, S.; Comisar, C. M. Fuel Cell Performance and Characterization of 1-D Carbon-Supported Platinum Nanocomposites Synthesized in Supercritical Fluids. *J. Catal.* **2008**, *259*, 5–16.
50. Dileo, R. A.; Castiglia, A.; Ganter, M. J.; Rogers, R. E.; Cress, C. D.; Raffaelle, R. P.; Landi, B. J. Enhanced Capacity and Rate Capability of Carbon Nanotube Based Anodes with Titanium Contacts for Lithium Ion Batteries. *ACS Nano* **2010**, *4*, 6121–6131.
51. Zhao, J.; Buldum, A.; Han, J.; Lu, J. P. First-Principles Study of Li-Intercalated Carbon Nanotube Ropes. *Phys. Rev. Lett.* **2000**, *85*, 1706–1709.